

# SUPERCONDUCTING RF-DIPOLE DEFLECTING AND CRABBING CAVITIES\*

S. U. De Silva<sup>#</sup>, J. R. Delayen

Center for Accelerator Science, Old Dominion University, Norfolk, VA 23529, USA.

Thomas Jefferson National Accelerator Facility, Newport News, VA 23606, USA.

## Abstract

Recent interests in compact deflecting and crabbing structures for future accelerators and colliders have initiated the development of novel rf structures. The superconducting rf-dipole cavity is one of the first compact designs with attractive properties such as high gradients, high shunt impedance, the absence of lower order modes, and widely separated higher order modes. Two rf-dipole cavities at 400 MHz and 499 MHz have been designed, fabricated and tested as proof-of-principle designs of compact deflecting and crabbing cavities for the LHC high luminosity upgrade and Jefferson Lab 12 GeV upgrade. The first rf tests have been performed on the rf-dipole geometries at 4.2 K and 2.0 K in a vertical test assembly with excellent results. The cavities have achieved high gradients with high intrinsic quality factors, and multipacting levels were easily processed.

## INTRODUCTION

The compact rf-dipole design consists of a cylindrically-shaped geometry with trapezoidal-shaped loading elements that was optimized from the rectangular-shaped geometry with racetrack-shaped loading elements [1, 2]. The optimized design shows improved properties with reduced and balanced peak surface electric and magnetic fields, high shunt impedance and widely separated higher order mode (HOM) spectrums. One of the key properties of the rf-dipole design is the non-existence on any lower order modes.

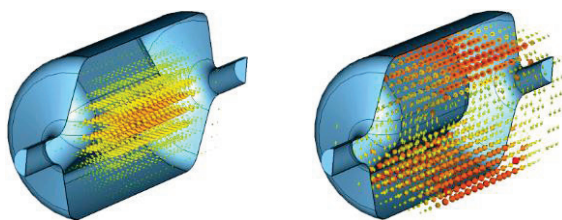


Figure 1: Electric field profile (left) and magnetic field profile (right) of the parallel-bar cavity.

The transverse momentum is primarily generated by the on-axis transverse electric and magnetic fields in the TE-like geometry shown in Fig. 1, which follows the Panofsky-Wenzel theorem [3]. The contribution from the transverse magnetic field is in opposition to, but much smaller in magnitude, than that of the transverse electric field.

## APPLICATIONS

The rf-dipole design was proposed as one of the rf separator options for the Jefferson Lab 12 GeV upgrade and as one of the crabbing cavity options for proposed LHC luminosity upgrade operating at 499 MHz and 400 MHz respectively. The first prototypes of the cylindrical-shaped 499 MHz and 400 MHz rf-dipole cavities shown in Fig. 2 have been fabricated and tested.

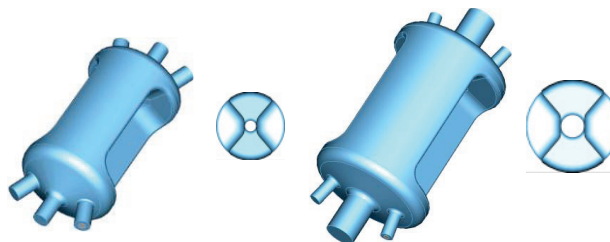


Figure 2: RF-dipole designs and cross sections of 499 MHz (left) and 400 MHz (right).

The rf properties of the proof-of-principle 499 MHz and 400 MHz rf-dipole cavities are given in Table 1.

Table 1: Properties of the 499 MHz and 400 MHz rf-dipole designs.

Parameter	499 MHz	400 MHz	Units
$\lambda/2$ of $\pi$ mode	300.4	374.7	mm
Cavity length	440.0	542.4	mm
Cavity diameter	242.2	339.9	mm
Aperture diameter ( $d$ )	40.0	84.0	mm
Bars length	260.0	350.3	mm
Bars inner height	50.0	80.0	mm
Angle	50.0	50.0	deg
Deflecting voltage ( $V_T^*$ )	0.3	0.375	MV
Peak electric field ( $E_P^*$ )	2.86	4.02	MV/m
Peak magnetic field ( $B_P^*$ )	4.38	7.06	mT
$B_P^* / E_P^*$	1.53	1.76	
Energy content ( $U^*$ )	0.029	0.195	J
Geometrical factor	105.9	140.9	$\Omega$
$[R/Q]_T$	982.5	287.0	$\Omega$
$R_T R_S$	$1.0 \times 10^5$	$4.0 \times 10^4$	$\Omega^2$
At $E_T^* = 1$ MV/m			

\* Authored by Jefferson Science Associates, LLC under U.S. DOE Contract No. DE-AC05-06OR23177. The U.S. Government retains a non-exclusive, paid-up, irrevocable, world-wide license to publish or reproduce this manuscript for U.S. Government purposes.

<sup>#</sup>sdesilva@jlab.org

### FABRICATION

The 499 MHz rf-dipole cavity was fabricated at Jefferson Lab [4] and the 400 MHz cavity by Niowave Inc. [5]. The 499 MHz cavity, of 3 mm thickness, consists of two end plates and the center piece formed with two shoulder blocks and two halves of the center shell as shown in Fig. 3-(a). The shoulder blocks were formed using Nb ingot and machined with additional thickness in order to reduce stresses at the bends.

The 400 MHz rf-dipole cavity was fabricated using 3 mm thick Nb sheets with a residual resistivity ratio (RRR) of 355-405. The cavity was formed with two end plates and the center piece, which was fabricated following a slightly different approach by forming the two halves of the center shell using a single set of dies.



Figure 3: Fabrication of (a) 499 MHz and (b) 400 MHz rf-dipole cavities.

In both rf-dipole cavities the frequency was adjusted by trimming the center shell.

### SURFACE TREATMENT AND ASSEMBLY

The cavities were processed at Jefferson Lab in preparation for the rf testing following the standard cavity processing procedure [6] as given below.

- Bulk removal of 120-150  $\mu\text{m}$  using BCP
- Heat treatment at 600  $^{\circ}\text{C}$  for 10 hours
- Light removal of 10-20  $\mu\text{m}$  using BCP
- High pressure rinsing

The complexity of the rf-dipole geometry resulted in non-uniform removal during the bulk BCP process as shown in Fig 4. The measurements were obtained from the Panametrics 25DL-Plus ultrasonic precision thickness gage with a resolution of 1  $\mu\text{m}$  and accuracy of  $\pm 10 \mu\text{m}$ , estimated with repeated measurements. The cavity was processed by a temperature controlled acid mixture in a closed vertical cabinet at 8  $^{\circ}\text{C}$  in order to minimize the absorption of hydrogen into the surface. The acid mixture was inserted from the bottom three ports and removed from the top three ports of the cavity, mounted vertically, using a manifold and circulated through the cavity in one direction. The processing was repeated 4 times with an expected removal of 30  $\mu\text{m}$  in each iteration and flipping the cavity vertically between the cycles, in order to obtain a uniform removal.

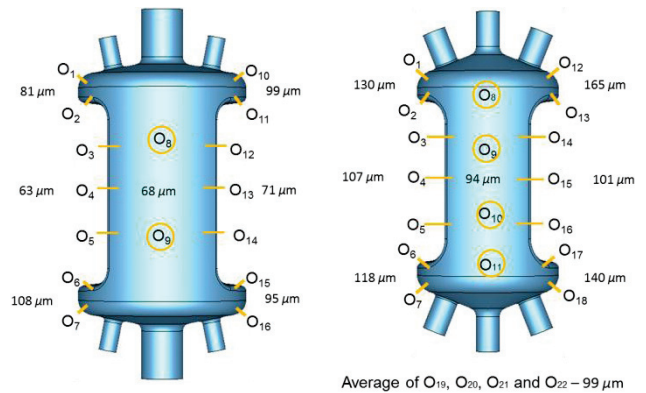


Figure 4: Average removal measured after the bulk BCP removal for the 400 MHz (left) and 499 MHz (right) rf-dipole cavities.

The 499 MHz cavity was processed for a duration of 15 minutes in each pass at an etch rate of 2.06  $\mu\text{m}/\text{min}$ , with an average removal of 108  $\mu\text{m}$  at the end of 4 passes. The 400 MHz cavity was processed for 17 minutes in 4 passes at a reduced etch rate of 1.8  $\mu\text{m}/\text{min}$  with an average removal of 81  $\mu\text{m}$ .

Both the 499 MHz and 400 MHz cavities were heat treated for 10 hours at 600  $^{\circ}\text{C}$  in a high-vacuum furnace for degassing of the hydrogen that was absorbed into the surface during the bulk BCP process. The partial pressure measured during the heating process for both the rf-dipole cavities are shown in Fig. 5.

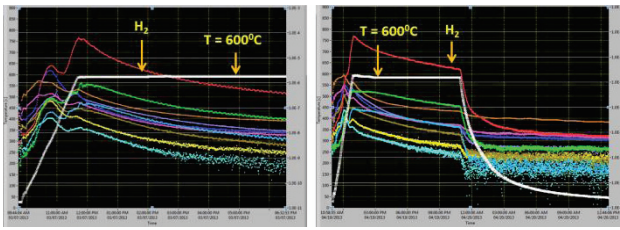


Figure 5: Furnace temperature and H<sub>2</sub> partial pressure level during high-vacuum heat treatment for the 400 MHz (left) and 499 MHz (right) rf-dipole cavities.

Following the heat treatment the cavities were etched again in a light BCP process to remove ~10 μm to eliminate the contamination due to the high-temperature heat treatment. Finally the cavity was high-pressure rinsed with ultra-pure water at a pressure of 1250 psi, prior to assembly. The cavities were assembled in a class 10 clean room with relief valves, fixed input coupler at the bottom and pick-up probe at the top of the cavity. No He processing or in-situ baking was performed.

### RF MEASUREMENTS

The rf-dipole cavities were tested in cw operation using a 500 W rf amplifier at both low power and high power. A series of vertical rf tests were performed at cryogenic temperatures of 4.2 K and 2.0 K in the vertical test facility at Jefferson Lab.

The performance was obtained by measuring the unloaded quality factor ( $Q_0$ ) as a function of the transverse voltage. Figures 6 and 7 show the measured unloaded quality factors at 4.2 K and 2.0 K as functions of the transverse electric field ( $E_t$ ), transverse voltage ( $V_t$ ), peak surface electric field ( $E_p$ ), and peak surface magnetic field ( $B_p$ ) for the 499 MHz and 400 MHz rf-dipole cavities.

#### 499 MHz Deflecting Cavity

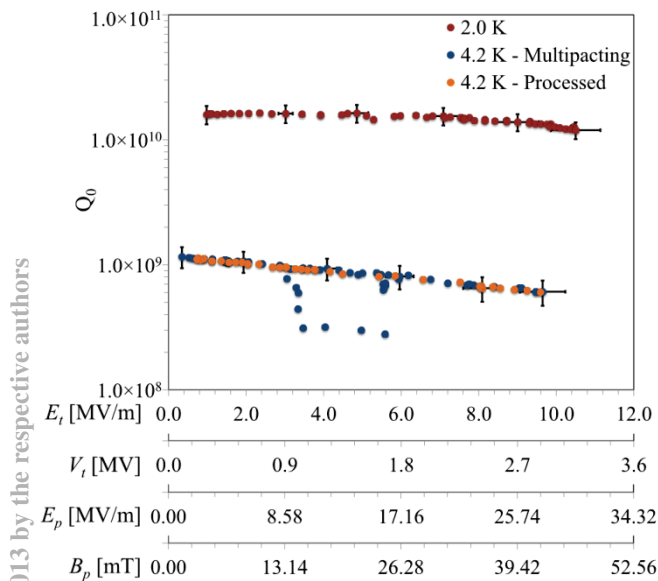


Figure 6: Quality factor at 4.2 K and 2.0 K rf tests for the 499 MHz rf-dipole cavity.

The  $Q$ -curves are relatively flat at both 4.2 K and 2.0 K with a  $Q_0$  above  $10^{10}$  at 2.0 K. The cavity experienced a hard quench around 10 MV/m of transverse electric field. At 2.0 K the cavity achieved peak electric field of 30 MV/m and a peak magnetic field of 46 mT at a transverse voltage of 3.15 MV. The cavity is reprocessed to investigate the quench will be retested. The currents results meet the design requirement of 5.6 MV can be achieved by two cavities.

#### 400 MHz Crabbing Cavity

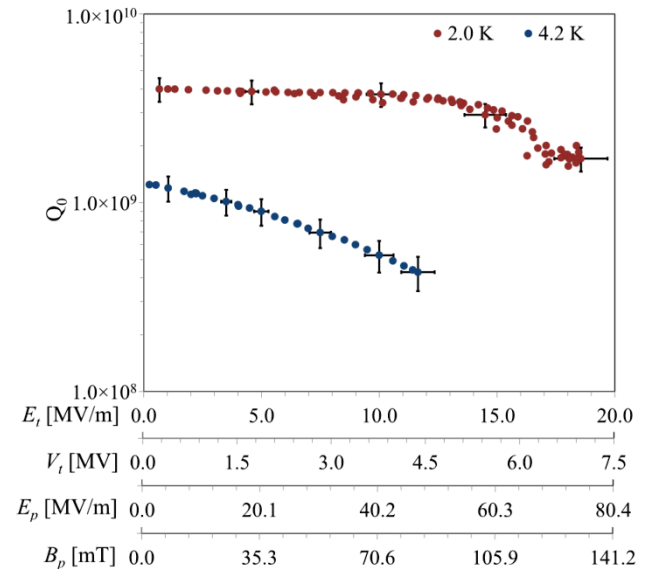


Figure 7: Quality factor at 4.2 K and 2.0 K rf tests for the 400 MHz rf-dipole cavity.

The  $Q$ -curves at 4.2 K shows a distinctive slope while it is relatively flat at 2.0 K. This is a fairly common feature that has been often observed in low-frequency superconducting cavities [7, 8]. Its origin is still poorly understood but possibly related to the heat transfer between Nb and liquid He. During the 4.2 K tests, the cavity achieved a transverse voltage of 4.35 MV that corresponds to a transverse deflecting field of 11.6 MV/m and was limited by the rf power available. The cavity was dissipating over 150 W at 11.6 MV/m.

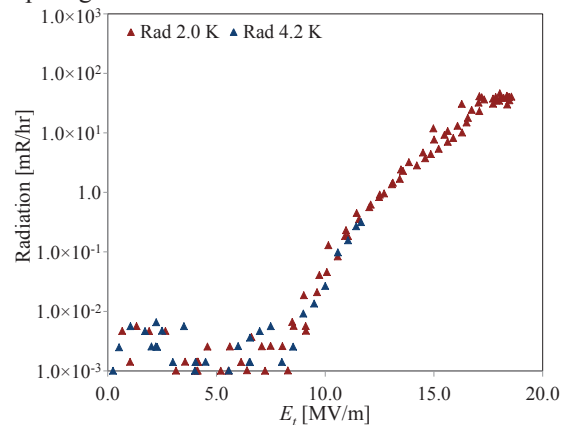


Figure 8: Field emission at 4.2 K and 2.0 K rf tests of the 400 MHz rf-dipole cavity.

At 2.0 K the cavity achieved a transverse voltage of 7.0 MV where a quench was observed. The Q-curve was flat until 5.0 MV and dropped possibly due to field emission. During the 2.0 K test the cavity reached cw peak surface fields of 75 MV/m and 131 mT. Higher levels of radiation were observed due field emission during the test at 2.0 K as shown in Fig. 8. The achieved cw voltage of 7.0 MV is twice the design voltage of 3.4 MV for the crabbing cavities for the proposed LHC High Luminosity upgrade [9].

### Multipacting

The multipacting levels were analysed for the rf-dipole cavities using the Track3P package from the SLAC ACE3P code suite [10] for an impact energy range of 20-2000 eV, which is the critical level in secondary emission for Nb [11].

Figure 9 shows the impact energies as a function of transverse voltage and order of the resonant particles. The resonant particles with impact energies resulting a secondary yield above 1.0 primarily lies at the end plates for the both the rf-dipole cavities.

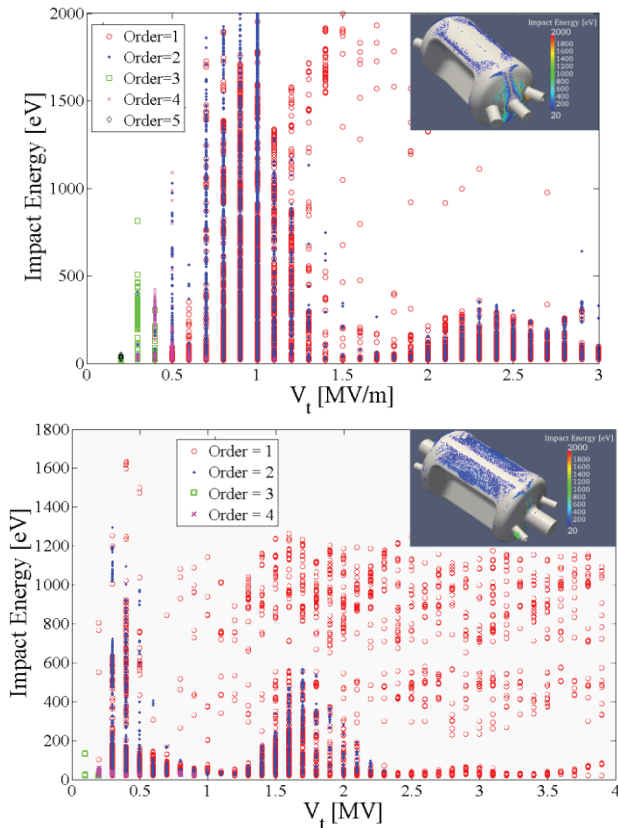


Figure 9: Impact energy with varying transverse voltage for 499 MHz (top) and 400 MHz (bottom) rf-dipole cavities.

During the first test of the 499 MHz rf-dipole cavity at 4.2 K multipacting levels were observed as shown in Fig. 6. The unloaded quality factor dropped at fields as low as 1.0 MV and continued until about 1.8 MV and  $Q_0$  recovered at increasing field levels. The multipacting

barrier observed is consistent with the simulated results as shown in Fig. 9. With repeated measurements at 4.2 K no multipacting levels reappeared.

In the first 2.0 K high power rf test a multipacting barrier was observed at very low fields for the 400 MHz rf-dipole cavity as well. After a few minutes the input power was increased, the multipacting level disappeared, and the transverse voltage jumped to about 2.5 MV. As shown in Figure 9, both the barriers were easily processed with increasing input power, and were shown to be soft multipacting barriers. This observation is consistent with what was expected from the simulations. The input power was then decreased down to 1 MV in small steps and no multipacting levels were observed. Further multipacting levels were not observed during the remainder of the 2.0 K test or on the following 4.2 K and 2.0 K tests.

### Surface Resistance ( $R_s$ )

The effective surface resistance ( $R_s$ ) was calculated by  $R_s = G/Q_0$  using the unloaded quality factor measured during the cavity cooling down process from 4.2 K to 2.0 K and the geometrical factor ( $G$ ). The measurements were obtained at very low input power that corresponds to 0.49–0.53 MV and 0.2–0.25 MV for the 499 MHz and 400 MHz cavities respectively. The measured data were fitted following the BCS theory [12] as shown in Fig. 10.

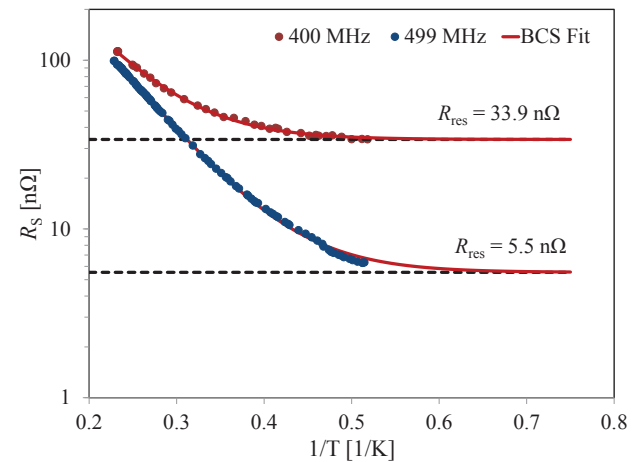


Figure 10: Effective surface resistance during the cavity cool down from 4.2 K to 2.0 K of the rf-dipole cavities.

The best fit of the data are given by,

$$R_s \text{ [n}\Omega\text{]} = \frac{2.6 \times 10^4}{T \text{ [K]}} \exp\left[-\frac{18.12}{T \text{ [K]}}\right] + 5.53 \quad (1)$$

for the 499 MHz cavity and

$$R_s \text{ [n}\Omega\text{]} = \frac{2.6 \times 10^4}{T \text{ [K]}} \exp\left[-\frac{18.67}{T \text{ [K]}}\right] + 33.9 \quad (2)$$

for the 400 MHz cavity. At 2.0 K the BCS resistances for 499 MHz and 400 MHz are 1.3 and 2.0 nΩ respectively. The low residual resistance of 5.5 nΩ in the 499 MHz cavity gives high unloaded quality factors.

The high residual resistance measured in the 400 MHz cavity is a result due to the surface losses at the beam

ports. The stainless steel blank flanges results in a power dissipation of 0.69 W. The corresponding  $Q_0$  due to the losses at the beam ports is  $3.8 \times 10^9$  which is consistent with the  $Q_0$  measured at 2.0 K.

### MULTI-CELL RF-DIPOLE CAVITIES

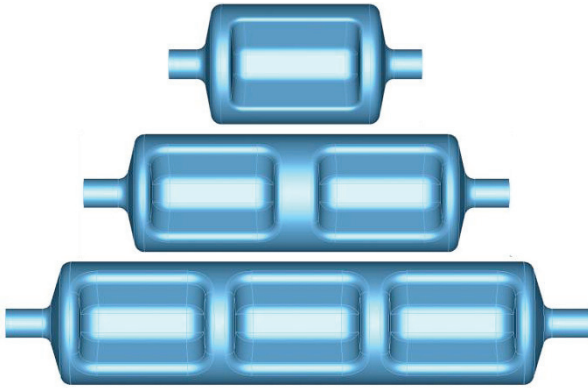


Figure 11: Single cell, 2 cell and 3 cell rf-dipole cavities of 400 MHz with a beam aperture of 84 mm.

The rf-dipole geometry easily supports multi-cell cavity designs as shown in Fig. 11, where the electric and magnetic field profiles for the deflecting and crabbing mode are shown in Fig. 12. The rf properties of a 2 cell and 3 cell rf-dipole cavity are given in Table 2 at 400 MHz frequency with a constant beam aperture of 84 mm.

The main advantage of the multi-cell designs is the reduced total cavity and cryomodule length. However multi-cell designs have similar order modes (SOM) with frequencies that are below the frequency of the fundamental deflecting and crabbing mode. The number of SOMs is directly related to the number of cells. For example, the 2 cell 400 MHz rf-dipole cavity has a SOM of 374.5 MHz and the 3 cell cavity has two SOMs with frequencies of 351.6 MHz and 376.8 MHz.

Table 2: Properties of the single cell, 2 cell and 3 cell 400 MHz rf-dipole cavities.

Parameter	Single cell	2 cell	3 cell	Units
Frequency		400		MHz
Aperture diameter		84.0		Mm
Cavity length	54.2	104.7	146.7	cm
Cavity diameter	34.0	34.5	35.4	cm
Bars length	35.0	34.5	34.5	cm
Bars inner height	80.0	85.0	85.0	mm
Angle	50.0	50.0	50.0	deg
Deflecting voltage ( $V_T^*$ )		0.375		MV
Peak electric field ( $E_P^*$ )	4.02	4.26	4.75	MV/m
Peak magnetic field ( $B_P^*$ )	7.06	7.4	7.77	mT
$B_P^* / E_P^*$	1.76	1.74	1.64	
Energy content ( $U^*$ )	0.195	0.114	0.079	J
Geometrical factor	140.9	127.8	131.8	$\Omega$
$[R/Q]_T$	287.0	488.4	708.1	$\Omega$
$R_T R_S$	$4.0 \times 10^4$	$6.2 \times 10^5$	$9.3 \times 10^4$	$\Omega^2$
At $E_T^* = 1$ MV/m				

The frequencies of the SOMs are close to the operating mode that requires to be damped well especially in high current applications.

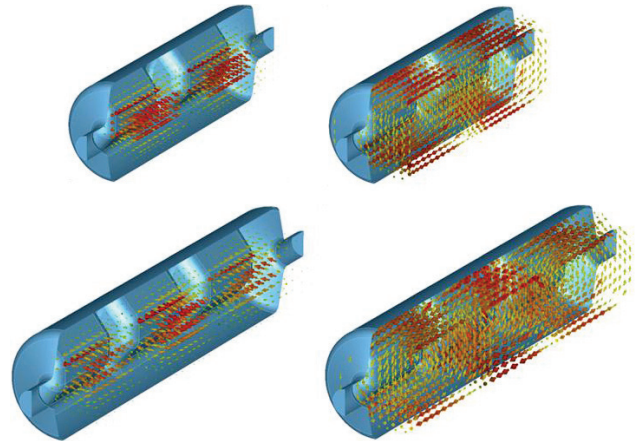


Figure 12: Electric field (left) and magnetic field (right) of 2 cell (top) and 3 cell (bottom) rf-dipole cavities.

### NEXT GENERATION OF RF-DIPOLE CAVITY

The LHC high luminosity upgrade requires crabbing systems that allows the head on collision of bunches in both horizontal and vertical planes [13]. The proof-of-principle 400 MHz rf-dipole cavity with cylindrical-shaped outer conductor does not meet the LHC crabbing cavity requirements in dimensional constraints, due to large transverse size. Therefore, the rf-dipole cavity was adapted into a squared-shaped outer conductor with fixed transverse dimensions where the frequency is adjusted by curving the edges as shown in Fig. 13. The work was done in collaboration with Zenghai Li at SLAC National Accelerator Laboratory. The rf properties of the cavity of the square-shaped cavity are shown in Table 3.

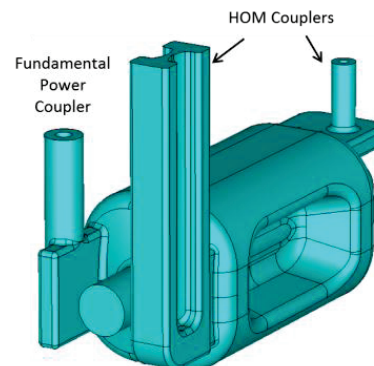


Figure 13: 400 MHz crabbing cavity proposed for LHC high luminosity upgrade.

The square-shaped rf dipole cavity is modified with curved loading elements to reduce the field non-uniformity and hence the multipole components. The reduction in the variation of the transverse voltage across the beam aperture is shown in Fig. 14. In comparison to a

similar design with flat loading elements the fields are uniform for a radius of 16 mm.

Table 3: Properties of the 400 MHz rf-dipole cavities with cylindrical-shaped and square-shaped and outer conductors.

Parameter	Cylindrical shaped	Square shaped	Units
Cavity length	542.4	556.2	mm
Cavity diameter	339.9	281.0	mm
Aperture diameter ( $d$ )	84.0	84.0	mm
Bars length	350.3	293.0	mm
Bars inner height	80.0	117.5	mm
Angle	50.0	~12.0	deg
<hr/>			
Deflecting voltage ( $V_T^*$ )	0.375	0.375	MV
Peak electric field ( $E_P^*$ )	4.02	3.65	MV/m
Peak magnetic field ( $B_P^*$ )	7.06	6.13	mT
$B_P^* / E_P^*$	1.76	1.68	
Energy content ( $U^*$ )	0.195	0.13	J
Geometrical factor	140.9	106.2	$\Omega$
$[R/Q]_T$	287.0	429.2	$\Omega$
$R_T R_S$	$4.0 \times 10^4$	$4.6 \times 10^4$	$\Omega^2$
At $E_T^* = 1$ MV/m			

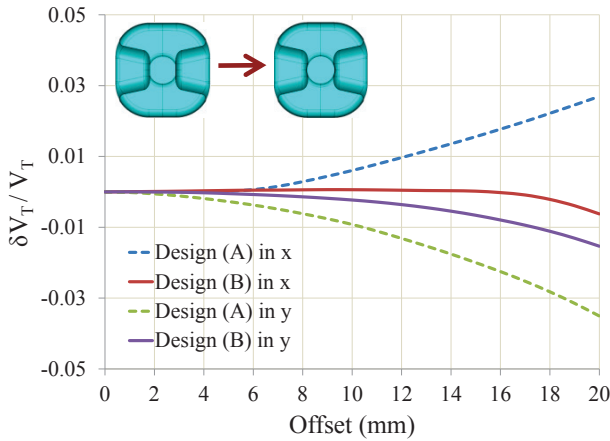


Figure 14: Normalized transverse voltage in x and y directions for the square shaped rf-dipole designs with (A) flat and (B) curved loading elements.

The cavity consists of fundamental power coupler and horizontal and vertical higher order mode couplers [14]. Figure 15 shows the ridged waveguide HOM coupler (a) and waveguide stub with coaxial coupler which is the vertical HOM coupler (b).

The horizontal HOM coupler damps horizontal deflecting modes, while the vertical HOM damps both vertical deflecting modes. Both these couplers supports in damping the accelerating modes. The asymmetric version of the vertical HOM coupler is modified to a symmetric shape specifically to damp the two vertical deflecting modes at 1.265 GHz and 1.478 GHz, with impedances above the transverse impedance threshold. With the modification the impedances are reduced by a factor of 10 as shown in Fig. 15 (c).

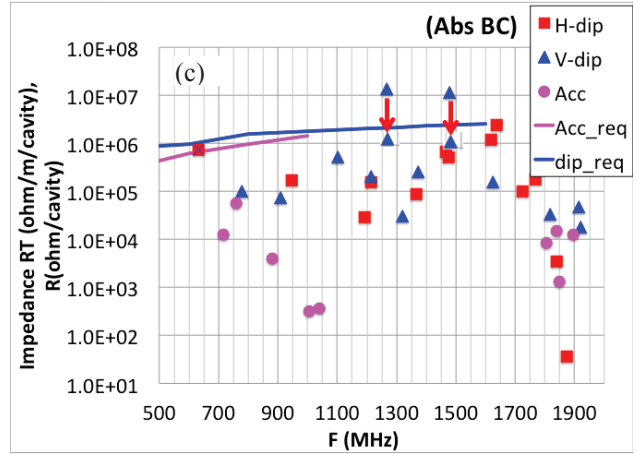
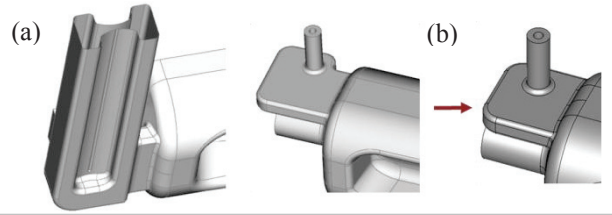


Figure 15: (a) Horizontal and (b) vertical higher order mode couplers with (c) impedance spectrum.

The multipacting levels in the square-shaped cavity have lesser impact compared to that of the cylindrical-shaped design. Higher levels are shown at the horizontal HOM coupler shown in Fig. 16. These critical multipacting levels are suppressed by slightly modifying the coupler by including a groove at the center [14].

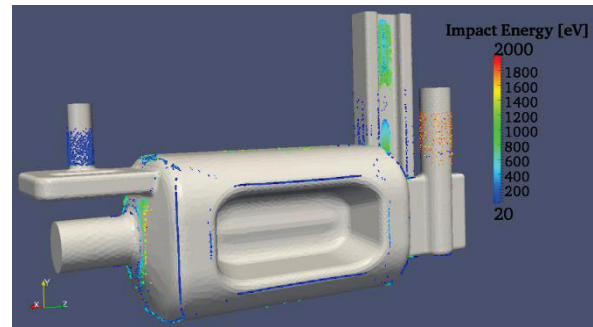


Figure 16: Impact energy of the resonant particles in the 400 MHz rf-dipole prototype.

## CONCLUSIONS

The rf-dipole cavity with trapezoidal-shaped loading is proven to have excellent properties such as low and balanced peak surface fields and high shunt impedance. The rf-dipole design also has attractive properties such as no lower order modes. This geometry provides compact designs at low operating frequencies. It is however limited in applications that require large beam apertures.

The first rf tests of the two proof-of-principle rf-dipole cavities of 499 MHz and 400 MHz were performed successfully and have demonstrated excellent rf properties at both 4.2 K and 2.0 K. The multipacting

levels were easily processed during the first tests for both the cavities and did not reoccur during the tests followed.

The 499 MHz deflecting cavity achieved high and uniform unloaded quality factors at 2.0 K. The cavity experienced a quench around 3.0 MV at both 2.0 K and 4.2 K. This could possibly due to a defects and further surface treatment are performed for retesting the cavity.

High surface electric and magnetic fields were achieved and high deflecting voltages were demonstrated in cw operation by the 400 MHz crabbing cavity. The relatively high residual surface resistance measured at 2.0 K was consistent with the power dissipated at the stainless steel flanges blanking the beam line ports. The rf test results obtained by the 400 MHz proof-of-principle rf-dipole cavity opens up possibilities of using these rf structures in future deflecting and crabbing applications.

### ACKNOWLEDGEMENTS

We want to give special thanks to HyeKyoung Park, Peter Kneisel, Tom Powers, and Kirk Davis of Jefferson Lab and Zenghai Li of SLAC. We want to acknowledge the help we have received from the Jefferson Lab SRF Institute for the processing of the cavity, and preparation for and conduct of the tests. We also would like to thank the help we have received from the Jefferson Lab Machine Shop during the fabrication of the 499 MHz cavity. This work was partially supported by the U.S. DOE through the US LHC Accelerator Research Program (LARP), by the EU FP7 HiLumi LHC Grant Agreement 284404, and by the U.S. DOE HEP SBIR/STTR program through Niowave Inc., Lansing, MI. This research used resources of the National Energy Research Scientific Computing Center, which is supported by the Office of Science of the U.S. DOE under Contract No. DE-AC02-05CH11231.

### REFERENCES

- [1] J. R. Delayen and H. Wang, Phys. Rev. ST Accel. Beams 12, 062002 (2009).
- [2] S. U. De Silva and J. R. Delayen, Phys. Rev. ST Accel. Beams 16, 012004 (2013).
- [3] W. K. H. Panofsky and W. A. Wenzel, Rev. Sci. Instrum. 27, 967 (1956).
- [4] H. Park, S. U. De Silva, and J. R. Delayen, in Proceedings of the 3<sup>rd</sup> International Particle Accelerator Conference, New Orleans, Louisiana (2012), p. 2450.
- [5] D. Gorelov, T. L. Grimm, S. U. De Silva, and J. R. Delayen, in Proceedings of the 3<sup>rd</sup> International Particle Accelerator Conference, New Orleans, Louisiana (2012), p. 2411.
- [6] P. Kneisel, Nucl. Instrum. Methods 557, 250 (2006).
- [7] J. R. Delayen, in Proceedings of the 25<sup>th</sup> Linear Accelerator Conference, Tsukuba, Japan (2010), p. 377.
- [8] M. Kelly, in Proceedings of the 13<sup>th</sup> Conference on RF Superconductivity, Beijing, China (2007), p. 44.

- [9] S. U. De Silva and J. R. Delayen, Phys. Rev. ST Accel. Beams 16, 082001 (2013).
- [10] K. Ko, A. Candel, L. Ge, A. Kabel, R. Lee, Z. Li, C. Ng, V. Rawat, G. Schussman, and L. Xiao, in Proceedings of the 25<sup>th</sup> Linear Accelerator Conference, Tsukuba, Japan (2010), p. 1028.
- [11] R. Calder, G. Dominichini, and N. Hilleret, Nucl. Instrum. Methods 13, 631 (1986).
- [12] J. Halbritter, Zeitschrift für Physik 266, 209 (1974).
- [13] P. Baudreghien, K. Brodzinski, R. Calaga, O. Capatina, E. Jensen, A. Macpherson, E. Montesinos, and V. Parma, Functional Specifications of the LHC Prototype Crab Cavity System, Tech. Rep. CERN-ACC-NOTE-2013-003 (CERN, 2013).
- [14] Z. Li, L. Ge, J. R. Delayen, and S. U. De Silva, in Proceedings of the 4<sup>th</sup> International Particle Accelerator Conference, Shanghai, China (2013), p. 2468.